16th World Conference on Earthquake, 16WCEE 2017

Santiago Chile, January 9th to 13th 2017

Paper N° 652

Registration Code: S-G1461735260

MODEL TESTING AND NUMERICAL ANALYSIS OF A METHOD FOR EVALUATION OF COASTAL PARAPET LEVEES' SEISMIC COEFFICIENTS CONSIDERING THEIR DYNAMIC CHARACTERISTICS

H. Fukawa[(1)], E. Kohama[(2)], R. Terada[(3)]

[(1)] *Researcher, Research and Development Center, Toa Corporation, Japan, h_fukawa@toa-const.co.jp*
[(2)] *Head, Earthquake and Structural Dynamics Group, Earthquake Disaster Prevention Engineering Department, Port and Airport Research Institute, Japan, kohama-e83ab@pari.go.jp*
[(3)] *Researcher, Earthquake and Structural Dynamics Group, Earthquake Disaster Prevention Engineering Department, Port and Airport Research Institute, Japan, terada-r852a@pari.go.jp*

Abstract

Methods for designing coastal parapet levees have not yet been developed for design seismic ground motion based on the Japanese design standard for port facilities, and no systems that consider the levees' dynamic characteristics have been built. This study used model testing and numerical analysis to establish a method for evaluating coastal parapet levees' seismic performance taking their dynamic characteristics under earthquake loads into consideration. Model tests using a shaking table were performed to examine the parapet levees' seismic responses to various design ground motions. Then the Fourier spectral ratios from the response accelerations of the ground surface and the structure were calculated to examine the levees' frequency characteristics. The acceleration response spectra at the ground surface were calculated to estimate the structures' maximum response accelerations. In addition, horizontal loading tests were conducted to verify the validity of the method of calculating natural frequencies. Seismic response and structural analyses were performed based on the configurations of the model tests. The applicability of the method for designing parapet levees was verified by comparing the results of the model tests and the numerical analyses.

Keywords: coastal parapet levees, model testing, numerical analysis, seismic coefficients, natural frequency

1. Introduction

Coastal parapet levees are structures with concrete walls designed to protect human life and property from high waves and tsunamis. They are installed behind the coastline when construction of a seawall near a shore is difficult due to the existence of coastal facilities like fishing ports.[1] In Japan, the performance of major harbor structures is evaluated using seismic coefficients calculated from structures' dynamic responses according to both ground conditions and design seismic motions determined at the engineering bedrock surface.[2] However, no clear design methods using the design seismic motions have yet been developed for varying coastal levee configurations, and no systems taking their dynamic characteristics into account have been built.

Several field surveys reported that some coastal parapet levees were heavily damaged in the 2011 off the Pacific Coast of Tohoku Earthquake. [3, 4] Since then, studies have examined how the tsunami loading after the earthquake finally lead to the structures' failure [5], but how the dynamic damage done to the structures by the earthquake before the tsunami arrived has not been made clear. The earthquake's effect cannot be excluded. It is necessary to understand the seismic performance of coastal parapet levees. This study aimed to establish a design method for evaluating parapet levees' seismic performance that considers their dynamic characteristics under earthquake conditions by model testing and numerical analysis.

Model testing was carried out using a shaking table to examine the seismic responses of parapet levees to various ground motions. Then natural frequencies were determined by both acceleration response spectra at the ground and Fourier spectral ratios between the ground and the parapet levees. Horizontal loading tests were also performed to calculate the natural frequency. Based on the results of the model testing, seismic response analysis and structural analysis were carried out. In the seismic response analysis, the natural frequencies were evaluated by the Fourier spectral ratio between the ground and the parapet levees. We also estimated their maximum acceleration from the response spectrum. In the structural analysis, a frame model with Winkler spring for piled pier design set forth in the Japanese design standards [2] was applied, and the applicability of the proposed method to the design of parapet levees was assessed.

2. Model shaking test

2.1 Experimental conditions

To examine the seismic behavior of parapet levees, model tests were carried out using a three-dimensional underwater shaking table at the Port and Airport Research Institute, Japan. Models simulated three parapet levee designs with different characteristics. Figure 1 shows the prototype and model cross-sectional dimensions of the structures. Type 1 has a pile foundation and T-type wall. It is located in the Tsugaruishikaigan fishing port in Iwate prefecture. [6] Type 2 also has a pile foundation and T-type wall, but its wall is higher and its piles are thicker than Type 1. It is planned to be constructed in the Atohama area of Ofunato port in Iwate prefecture.[7] Type 3 has a spread foundation and gravity-type wall, as specified in the Japanese design standards.[1] Table 1 shows the experimental conditions. Case 1, Case 3, and Case 4 have dense ground (D_r=80%), while Case 2 has loose ground (D_r=50%). Figure 2 shows the plan view and cross-section of Case 1. The ground was formed using Iide silica sand (No. 6, average grain size of about 0.3 mm), and placed using the air pluviation method in order to make the soil layers have the prescribed density. The parapet model to be monitored was set in the center of the tank, with dummy parapet models on either side. The placed ground was 4.0 m long, 1.0 m deep and 1.4 m wide. Two cases at a time (Cases 1, 2 and Cases 3, 4) were carried out simultaneously using a rigid tank 4.0 m long, 2.8 m wide, and 1.5 m deep with a center partition.

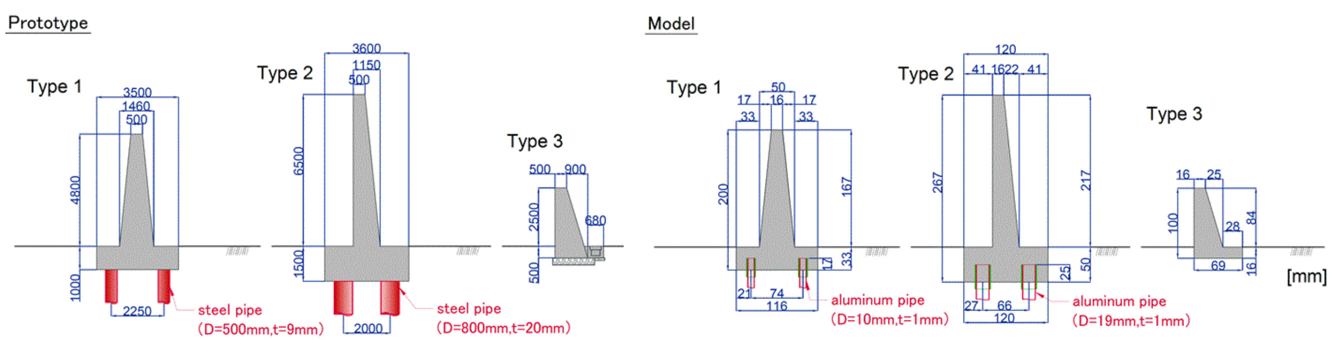

Fig.1 – Parapet levee cross-sections

Table 1 – Experimental cases

Experimental case	Levee type		Ground condition (D_r)
Case 1	pile foundation and T-type wall	(Type 1)	dense (80%)
Case 2	pile foundation and T-type wall	(Type 1)	loose (50%)
Case 3	pile foundation and T-type wall	(Type 2)	dense (80%)
Case 4	spread foundation and gravity-type wall	(Type 3)	dense (80%)

The scale ratio λ (prototype/model) was set at 30 based on the sizes of the prototypes and testing chamber. Similarity rules for 1G conditions suggested by Iai [8] were applied. Table 2 shows the similarity ratios. Materials and scales were set in order to make the flexural rigidity of the piles satisfy the similarity rules. Aluminum (A1070) was selected and the second moments of area were calculated by Eq. (1). Table 3 shows the pile characteristics.

$$I = \frac{\pi}{64}\left(D^4 - t^4\right) \tag{1}$$

D is the pile diameter (mm), t is the pile thickness (mm), and I is the second moment of area (mm^4).

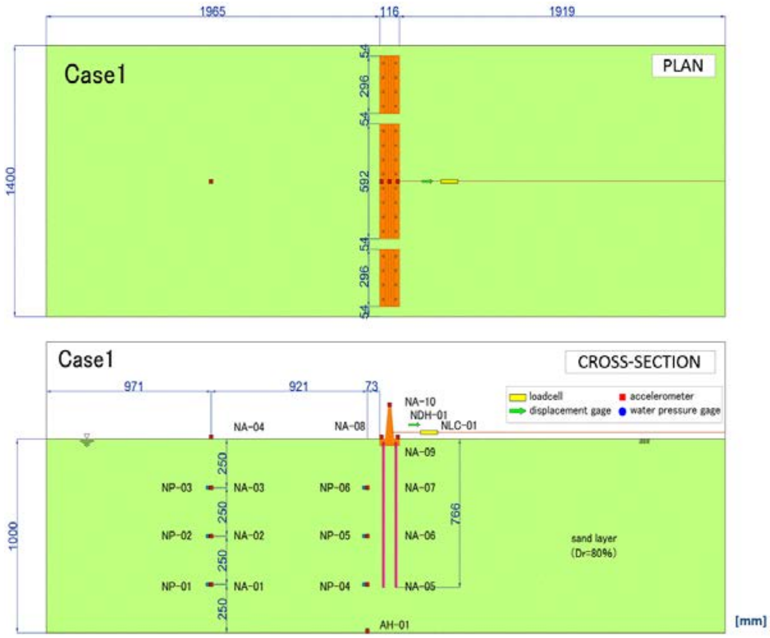

Fig. 2 – Experiment setup plan and cross-section

Table 2 – Similarity rules and scale

Measurement	Scaling factors (prototype/model)	Scale (λ=30)
length	λ	30
density	1	1
time	$\lambda^{0.75}$	12.8
stress	λ	30
pore water pressure	λ	30
displacement	$\lambda^{1.5}$	164
acceleration	1	30
strain	$\lambda^{0.5}$	5.48
rate of pore water flow	$\lambda^{0.75}$	12.8
flexural rigidity	$\lambda^{4.5}$	4,436,553
longitudinal rigidity	$\lambda^{2.5}$	4,930

Table 3 – Pile characteristics

Levee type	Experimental case	Scale	Outer diameter	Thickness	Moment of inertia	Elastic modulus*	Flexural rigidity
			D	t	I	E	EI
			mm	mm	mm^4	kN/m^2	kNm^2
Type 1	Case 1 Case 2	prototype	500	9	4.18×10^8	2.00×10^8	8.37×10^4
		model	10	1	2.90×10^2	7.03×10^7	0.0204 (9.04×10^4)**
Type 2	Case 3	prototype	800	20	3.73×10^9	2.00×10^8	7.46×10^5
		model	19	1	2.30×10^3	7.03×10^7	0.162 (7.17×10^5)**

*prototype : iron, model : aluminum
**prototype scale

2.1.1 Shaking test

The shaking tests used nine input waves with varying characteristics. [9] Their time histories are shown in Figure 3. The Mito, Ofunato, Kobe, Miyazaki, and Hachinohe waves are observed seismic motions, and the others are simulated strong motions evaluated taking fault movements into account. The waves' time scale was compressed according to the similarity rules ($1/30^{0.75}$=1/12.8).

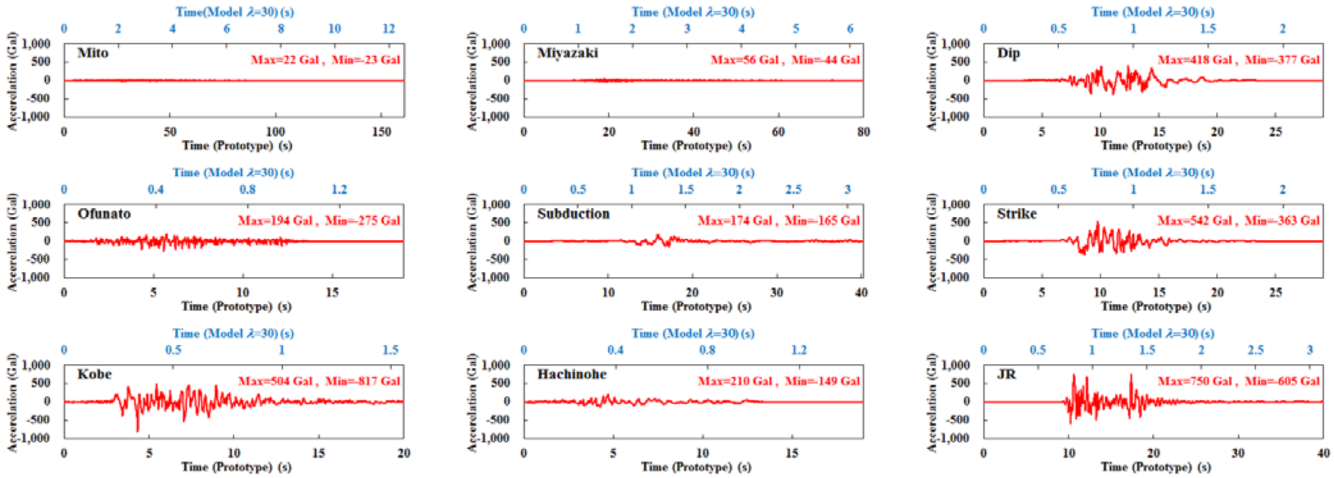

Fig. 3 – Time histories of input waves

2.1.2 Horizontal loading test

Before and after the shaking tests, horizontal loading tests were carried out to examine the natural frequencies of the parapet levees. Before each shaking test, a load was applied until a tiny displacement occurred (~0.01mm) as there was some apprehension about the ground distribution. After each shaking test, load was applied, continuing until the maximum load was attained or the wall fell. Figure 4 is a schematic view of the horizontal loading test. Horizontal force was applied at the wall's center of gravity using a wire rope by placing sand weights into a container. The horizontal load was measured by a load cell attached to the rope, and horizontal displacement was measured with a laser gauge.

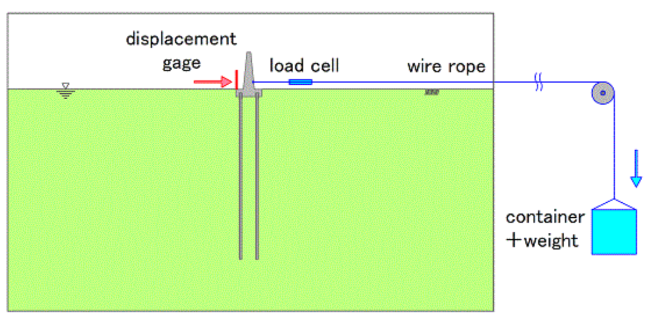

Fig. 4 – Schematic view of horizontal loading test

2.2 Experimental results

2.2.1 Seismic responses of parapet levee and ground

Figure 5 shows the location of the accelerometers on the model. Horizontal acceleration was measured by three gauges for the T-type wall (Type 1, Type 2), and two gauges for the gravity-type wall (Type 3). The acceleration at the center of gravity was calculated by Eq. (2), taking the location into consideration. Rotation acceleration at the levee's center of gravity was calculated by the gap acceleration at the center of gravity using the upper and lower accelerations as in Eq. (3). Rotation acceleration was divided by the height of the center of gravity as in Eq. (4), yielding angular acceleration (Gal/m).

$$Acc._{GravityCenter} = \frac{H_1}{H} Acc._{Upper} + \frac{1}{2}\frac{H_2}{H} Acc._{Lower1} + \frac{1}{2}\frac{H_2}{H} Acc._{Lower2} \tag{2}$$

$$RotationAcc._{GravityCenter} = \frac{\left(Acc._{Upper} - Acc._{Lower}\right)}{\left(H/H_1\right)} \tag{3}$$

$$AngularAcc._{GravityCenter} = \frac{RotationAcc._{GravityCenter}}{H_1} \tag{4}$$

$Acc._{\mathrm{GravityCenter}}$ is the horizontal acceleration at the wall's center of gravity (Gal), $Acc._{\mathrm{Upper}}$ is the horizontal acceleration at the upper part of the wall (Gal), $Acc._{\mathrm{Lower}}$ is the horizontal acceleration at the lower part of the wall (Gal), $RotationAcc._{\mathrm{GravityCenter}}$ is the rotation acceleration at the wall's center of gravity (Gal), $AngularAcc._{\mathrm{GravityCenter}}$ is the angular acceleration at the wall's center of gravity (Gal/m), H is total height (cm), H_1 is the height from the center of gravity to the lower part (cm), and H_2 is the height from the upper part to the center of gravity (cm).

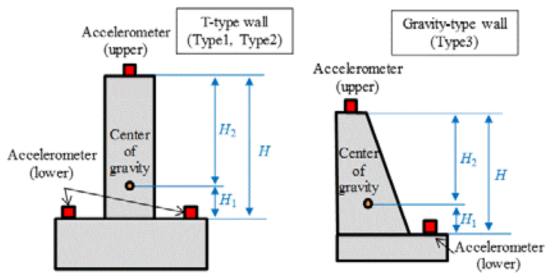

Fig. 5 – Accelerometer locations

Figure 6 shows the results of the shaking test. Figure 6(a) shows the relationship between the maximum accelerations of the input wave and at the wall's center of gravity. Figure 6(b) shows the relationship between the maximum input acceleration and angular acceleration. The figures also include the names and shaking orders of the input waves. In Figure 6(a), the maximum acceleration at the center of gravity for Case 2 is clearly smaller than Case 1. The excess pore water pressure ratio for the Kobe wave of Case 2 rose to 0.7, which affected the acceleration response. In Figure 6(b), a large angular acceleration appeared for the spread foundation of Case 4. Otherwise there were relatively small angular accelerations for pile foundations.

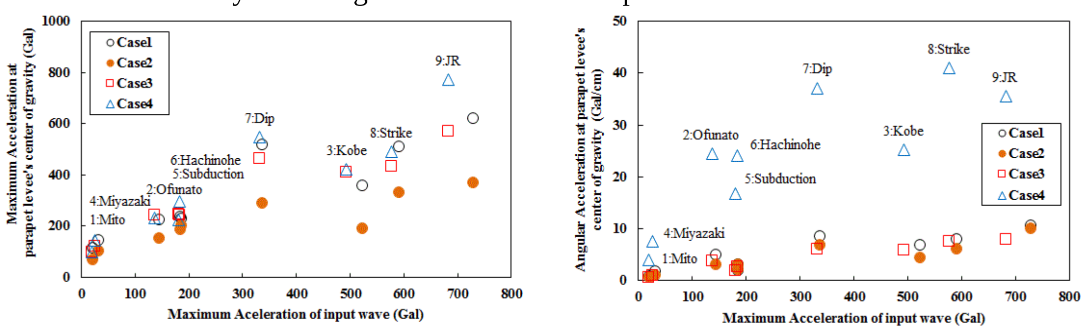

(a) Input acc. vs Center of gravity acc.
(b) Input acc. vs Angular acc.

Fig. 6 – Shaking test results

2.2.2 Vibration characteristics of parapet levees

Figure 7 shows the relationship between horizontal load and displacement from the horizontal loading test. The figure shows two extended initial gradients before and after shaking. Frequencies in the figure are written at the prototype scale. The initial gradient of Case 1 was a little larger than Case 2, because of its dense ground. Case 3, which has larger piles, also had a large initial gradient due to its solid structural resistance to horizontal loads. The spread foundation type (Case 4) fell down after the shaking test. It had less resistance against horizontal loads than the other cases because it has no piles and shallow footings. The natural period T_s (natural frequency: $1/T_s$) was calculated by Eq. (5), using the initial gradient as the elastic constant of the structure.

$$T_s = 2\pi\sqrt{\frac{W}{gK}} \tag{5}$$

T_s is natural period of the structure (s), W is weight and vertical load (kN), g is gravity acceleration, and K is the horizontal spring constant of the structure (kN/m).

Before the shaking tests, Case 3 had the largest elastic constant and natural frequency. After the shaking, its natural frequency was almost unchanged. On the other hand, the natural frequencies after shaking for Cases 1, 2, and 4 were slightly larger than those observed before shaking.

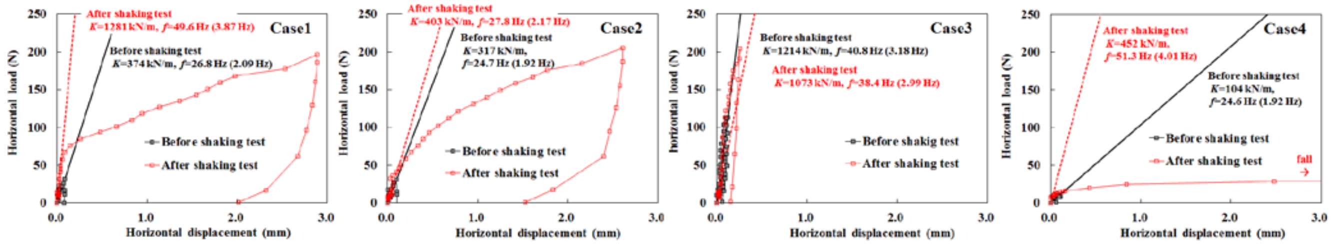

Fig. 7 – Relationship between horizontal load and horizontal displacement

Natural frequencies were also calculated from the Fourier spectral ratios between the ground surface and parapet wall. The spectra were smoothed with Parzen's spectrum window (bandwidth: 0.3 Hz) and moderate spectral ratio peaks were picked as the natural frequencies. Figure 8 shows the natural frequencies, where the horizontal axis is the maximum acceleration at the base of the shaking table. The figure also shows the order of the shaking tests, and the natural frequencies from the horizontal loading tests are shown as horizontal lines. The natural frequencies evaluated from the spectral ratios were smaller for large accelerations because the stiffness of the ground decreased, associated with larger excitation. The natural frequencies calculated from the horizontal loading test were very similar to those obtained from the spectral ratio with maximum base acceleration lower than 200 Gal. Horizontal loading tests focus on static forces and fine structure displacements, so they might be valid for estimating natural frequencies for small acceleration conditions. However, the differences between the natural frequencies were larger under large seismic conditions, because the natural frequencies obtained from the peak spectral ratios decreased.

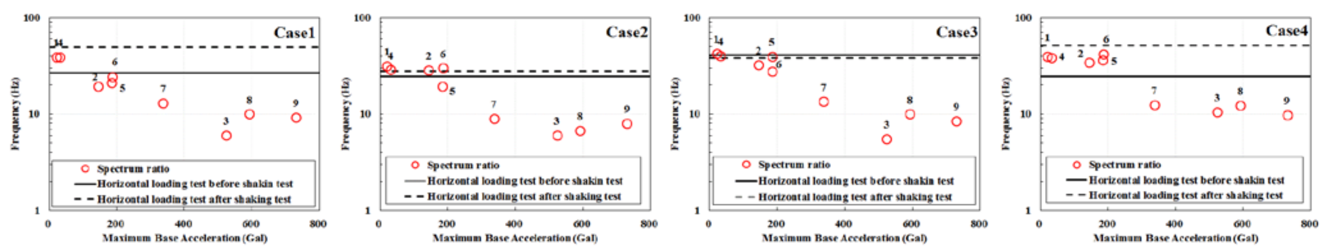

Fig. 8 – Comparison of natural frequencies

2.2.3 Estimation of maximum acceleration response using response spectra

Figure 9 compares maximum accelerations estimated by the response spectra and measured at the parapet levees' center of gravity in the shaking tests. Response spectra were calculated from time histories at the ground surface, and damping ratios were set at 5% increments up to 55%, with natural frequencies from the spectral ratio used for estimation. The estimated and measured accelerations were strongly correlated at damping ratios from 40% to 55%, and the errors between the two were less than 100 Gal.

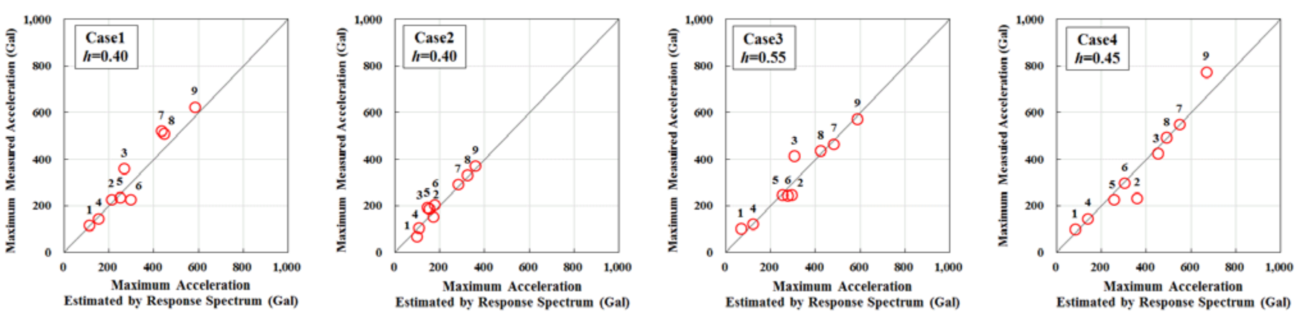

Fig. 9 – Relationship between the maximum estimated and measured accelerations

3. Numerical analysis

3.1 Flow of numerical analysis

Figure 10 shows the analysis flow, where two-dimensional seismic response and structural analyses were performed focusing on the pile foundations. As in the shaking model test, natural frequencies were obtained from the peak Fourier spectral ratios between the free field ground surface and the levee's center of gravity. We compared the maximum accelerations estimated from the response spectrum at the free field surface and those from the seismic response analysis. In the structural analysis, natural frequencies were calculated from the elastic constants in the same way as for the horizontal loading tests. We also related the natural frequencies obtained from the structural analysis to the response spectra, and estimated maximum acceleration responses.

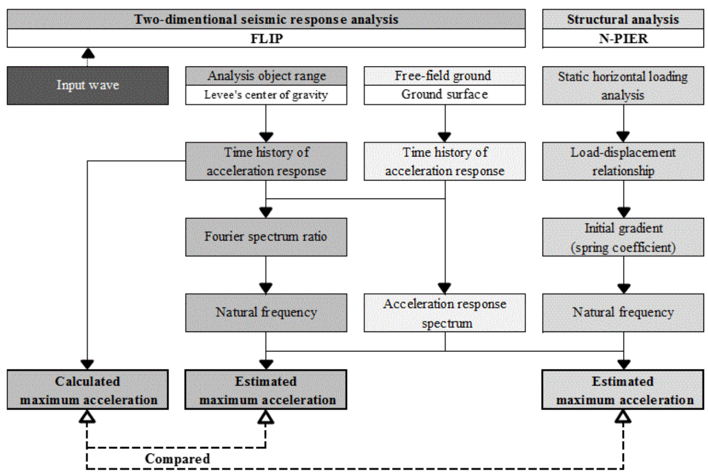

Fig.10 – Numerical analysis flow

3.2 Numerical analysis conditions

3.2.1 Seismic response analysis

FLIP, a finite element analysis program for liquefaction processes, was used for the seismic response analysis. [10, 11] The cross-sections and the parameters are shown in Figure 11 and Table 4. Structural and ground parameters were based on the models used by Nagao et al. [9] in a study of seismic designs for piers. Interacting spring elements were set between the piles and the ground, and parameters for one unit of depth were used for pile elements. Ground parameters were set for three conditions without liquefaction, as per the standard method suggested by Morita et al. [12] The 9 types of input waves [9] were used at the prototype time scale. The Rayleigh damping constant β was set as 0.002, considering the natural period and displacement of the ground during excitation.

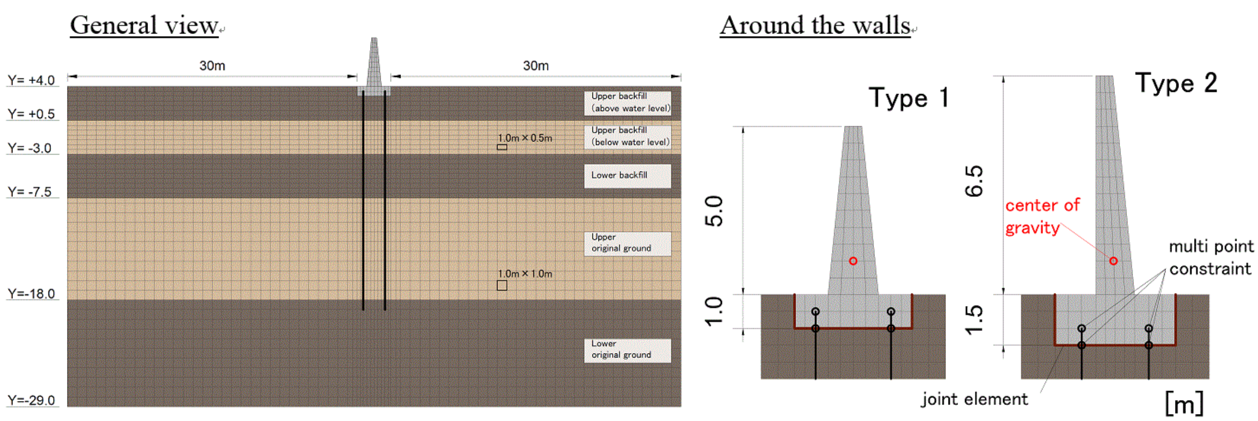

Fig.11 – Cross-sections for seismic response analysis

Table 4 – Parameters for seismic response analysis

(a) Ground element

Ground condition	Layer		Wet density	Standard effective confining pressure	Standard initial shear modulus	Standard initial bulk modulus	Cohesion	Angle of internal friction	Maximum damping constant	Shear wave velocity	N-value	Note
			t/m^3	kN/m^2	kN/m^2	kN/m^2	kN/m^2	°	-	m/s		
Ground 1	backfill	upper (above water level)	1.8	89.8	25,920	67,595	0	37	0.24	120	3	Classified into the ground type III (natural period is about 1.20s)
		upper (below water level)	2.0									
		lower										
	original ground	upper	2.0	239.8	45,000	117,353	0	38	0.24	150	6	
		lower										
Ground 2	backfill	upper (above water level)	1.8	89.8	58,320	152,089	0	38	0.24	180	10	Classified into the ground type II (natural period is about 0.80s)
		upper (below water level)	2.0									
		lower										
	original ground	upper	2.0	198.5	72,200	188,286	0	38	0.24	190	12	
		lower		279.2	125,000	325,980	0	39	0.24	250	28	
Ground 3	backfill	upper (above water level)	1.8	72.9	79,380	207,011	0	38	0.24	210	15	Classified into the ground type I (natural period is about 0.60s)
		upper (below water level)	2.0									
		lower		142.3	125,000	325,980	0	39	0.24	250	28	
	original ground	upper	2.0	198.5	156,800	408,910	0	39	0.24	280	39	
		lower		279.2	405,000	1,056,176	0	44	0.24	450	50	

(b) Pile element

Levee type	Outer diameter	Thickness	Yield stress	Moment of inertia	Cross sectional area	Full plastic moment	Momental rigidity First gradient	Momental rigidity Secondary gradient	Yield axis direction force	Note
	m	mm	N/mm^2	m^4	m^2	kNm	kNm^2	kNm^2	kN	
Type 1	0.5	9	315 (SKK490)	418×10^{-6}	1388×10^{-5}	684	8.36×10^4	0	4372	Depth : 2.25m (one pile unit)
			315 (SKK490)	186×10^{-6}	617×10^{-5}	304	3.34×10^4	0	1943	Depth : 1.00m
Type 2	0.8	20	235 (SKK400)	3730×10^{-6}	4091×10^{-5}	2860	7.46×10^5	0	11517	Depth : 2.00m (one pile unit)
			235 (SKK400)	1865×10^{-6}	2451×10^{-5}	1430	3.73×10^5	0	5759	Depth : 1.00m

(c) Joint element

Location	Initial compression stiffness	Initial shear stiffness	Cohesion	Frictional angle	Note
	kN/m^2	kN/m^2	kN/m^2	°	
Side	1.0×10^6	0	0	15	
Bottom	1.0×10^6	1.0×10^6	0	31	

3.2.2 Structural analysis

The N-Pier program was used for structural analysis. The models and parameters are shown in Figure 12. Three ground conditions were adapted to match the seismic response analysis. Since the ground surface was set at the footing's bottom level due to the program constitution, the confining pressure was corrected by adding a vertical load on the ground surface equivalent to the footing height.

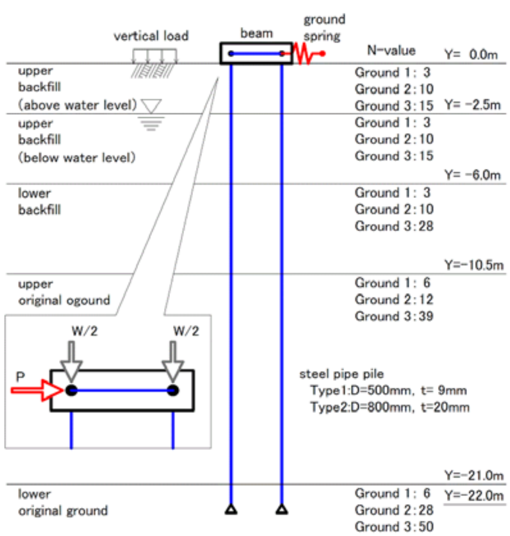

Fig.12 – Schematic view of structural analysis

The methods and conditions for the structural analysis are shown in Table 5. The subgrade reaction was represented by the springs connected to the pile elements, whose coefficient was calculated by the two methods shown in Table 5(a). One is the method from the Japanese standard for harbor facilities [2] called [Standard 1] here, and the other is the method from the Japanese standard for highway bridges [13, 14] called [Standard 2].

While [Standard 1] estimates the coefficient of subgrade reaction directly from the N-value, [Standard 2] considers elastic modulus E, diameter D, and a characteristic value β of the piles evaluated from the N-value. Furthermore, other conditions were taken into consideration using the coefficient α and the existence of the ground spring connected to the footing. Coefficient α is commonly used to estimate ground resistance in Japanese structural design. This coefficient changes depending on the assumed design conditions. It is usually set as 1.0 for static conditions or 2.0 for seismic conditions. [13] Structural analyses were carried out on the 8 conditions shown in Table 5(b). The natural frequencies were calculated from the initial gradient between the horizontal load and the horizontal displacement of the wall, using Eq. (5), which is the same as the experimental horizontal loading test.

Table 5 – Structural analysis conditions

(a) Calculation methods for subgrade reaction

Coefficient of horizontal ground resistance K_H	Reference	Coefficient of resistance from ground spring K_H	Reference
$K_H=\alpha 1500N$	Standard 1	$K_H = K_{H0}\left(\frac{B_H}{0.3}\right)^{-3/4}$ $K_{H0} = \frac{1}{0.3}\alpha E_0$ $E_0 = 2800N$ $B_H = \sqrt{A_H}$	Standard 2
$K_H = K_{H0}\left(\frac{B_H}{0.3}\right)^{-3/4}$ $K_{H0} = \frac{1}{0.3}\alpha E_0$, $E_0 = 2800N$ $B_H = \sqrt{D \cdot \frac{1}{\beta}}$, $\beta = \sqrt[4]{\frac{K_H D}{4EI}}$	Standard 2		

(b) Calculation conditions

Calculation condition	Method	Ground resistance to the footing	Coefficient
Cond.1	Standard 1	nothing	α=1.0
Cond.2	Standard 1	ground spring	α=1.0
Cond.3	Standard 1	nothing	α=2.0
Cond.4	Standard 1	ground spring	α=2.0
Cond.5	Standard 2	nothing	α=1.0
Cond.6	Standard 2	ground spring	α=1.0
Cond.7	Standard 2	nothing	α=2.0
Cond.8	Standard 2	ground spring	α=2.0

3.3 Numerical analysis results

3.3.1 Parapet levee and ground seismic responses

Figure 13 shows the results of the seismic response analysis. Figure 13(a) shows the relationship between the maximum accelerations of the input waves and the wall's center of gravity. Acceleration at the center of gravity increased for large input accelerations. At levels above 400 Gal of input acceleration, there were especially large responses for Type 2. Figures 13(b) and (c) show the relationship between the maximum accelerations at the ground surface and the center of gravity. Figure 13(b) shows the results of the numerical analysis (FLIP). In that analysis, the acceleration response at the center of gravity was 1.5 to 2.0 times as large as at the ground surface for Type 2, but only 1.0 to 1.5 times for Type 1. On the other hand, in the shaking tests of Figure 13(c), there were no remarkable differences in maximum acceleration among the levee types. Figure 13(d) shows the relationship of the maximum values of the input acceleration and angular acceleration at the center of gravity. Also in this figure, the angular acceleration for Type 2 is very high at a base acceleration of larger than 400 Gal. It seems that Type 2 parapet levees rotated easily under large seismic loads in the numerical analysis, and the large horizontal acceleration at the center of gravity was caused by the rotation behavior of the parapet wall.

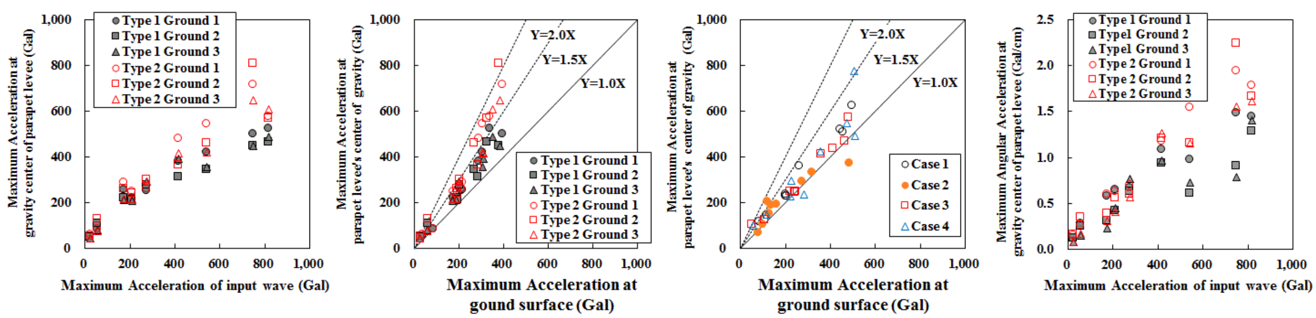

(a) Base vs center of gravity acc.

(b) Ground surface vs center of gravity acc. (FLIP)

(c) Ground surface vs center of gravity acc. (Shaking test)

(d) Input vs Angular acc.

Fig.13 – Seismic response analysis results

3.3.2 Vibration characteristics of parapet levees

Natural frequencies calculated by the two different methods, N-Pier and FLIP, are shown in Figure 14. The horizontal axis is the maximum acceleration at the levee's center of gravity. The natural frequencies calculated by FLIP's spectral ratios decreased in large accelerations, because FLIP simulated the reduction of soil rigidity considering its non-linear characteristics well. On the other hand, the natural frequencies of the structural analysis stayed constant without regard to acceleration. Among the conditions in table 5(b), Condition 1 calculated minimum frequencies, and Condition 8 calculated maximum frequencies. Comparing the standards for subgrade reaction, Standard 2 calculated larger frequencies than Standard 1, and the ground spring connecting to the footing enhanced the subgrade reaction. As a result, natural frequencies varied by 2 to 3 times depending on the analysis conditions.

The natural frequencies for Type 1, calculated by the FLIP's spectral ratios, were close to the frequencies calculated by the structural analysis under 300 Gal, as shown in Figure 14. The values calculated in the structural analysis nearly adequate at small accelerations. However, the natural frequencies from the structural analysis for Type 2 were relatively high, and did not fit the natural frequencies of the spectral ratio. The structural analysis focused on the nodal points of the beam, and calculated the natural frequencies using the beam's displacement. Thus, the structural analysis indicates that it would more difficult to produce horizontal movement than seen for real walls, particularly in the case of tall parapet walls like Type 2 which have high centers of gravity. As a result, Type 2 had relatively high frequencies as calculated by the structural analysis.

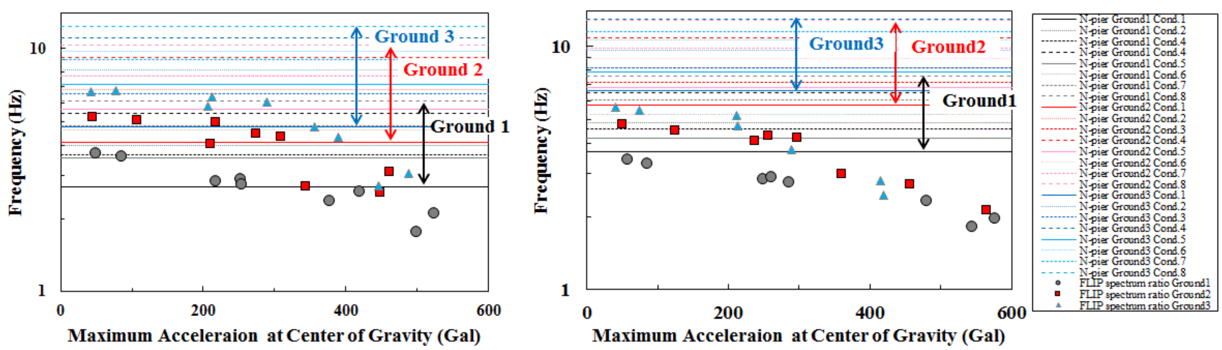

Fig.14 – Comparison of natural frequencies

3.3.3 Estimation of parapet levee's maximum accelerations from response spectra

The relationship of the maximum accelerations estimated by the acceleration response spectra at the free field ground surface to those measured at the parapet levees' centers of gravity is shown in Figure 15. The figure also shows whether the natural frequency was determined by the spectrum ratio or the structural analysis with a prescribed condition. The difference between them was smallest when the damping constant used to calculate the response spectrum was 50% for Type 1 and 30% for Type 2. The acceleration response spectra at the free field ground surface on Ground 2 are shown in Figure 16, which shows three natural frequencies and the maximum acceleration of the parapet wall.

For Type 1, maximum accelerations estimated by the response spectra using the natural frequencies of the spectral ratio corresponded reasonably well with those calculated by the seismic response analysis as shown in Figure 15. The error was also small for frequencies calculated by the structural analysis for both conditions 1 and 8. In Figure 16, for the JR wave and Type 1, the maximum acceleration of the center of gravity is close to the spectrum with a 0.50 damping constant. Although there was a span of about 8 Hz between the natural frequencies, gaps in the response spectrum did not appear, because of the flat shape of the spectrum. Therefore, the maximum acceleration of Type 1 levee could be estimated correctly.

On the other hand, for Type 2 in Figure 15, estimation errors are larger than for Type 1 for both the spectral ratio and the structural analysis methods, and there were particularly great disparities with large accelerations over 500 Gal. In Figure 16, a value of 0.30 for the damping constant *h* produced the lowest errors overall for the Hachinohe wave, but at that level, the spectrum of the JR wave is underestimated. This might be the result of rocking behavior by the wall, but this large acceleration for Type 2 did not occur in the experiments on Case 3 in Figure 13. The inconsistency in seismic behavior of the parapet levees between the experiments and analyses needs to be studied in detail.

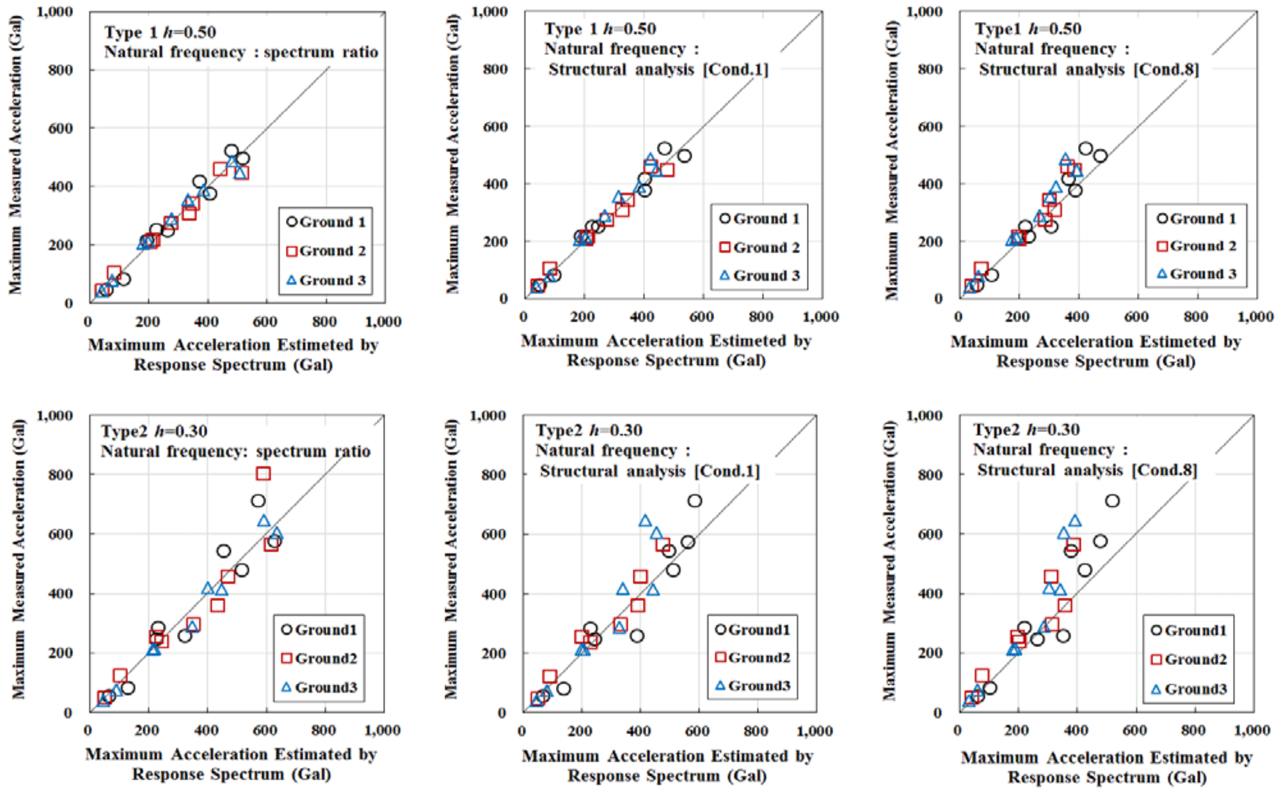

Fig.15 – Relationship of estimated and analyzed maximum accelerations

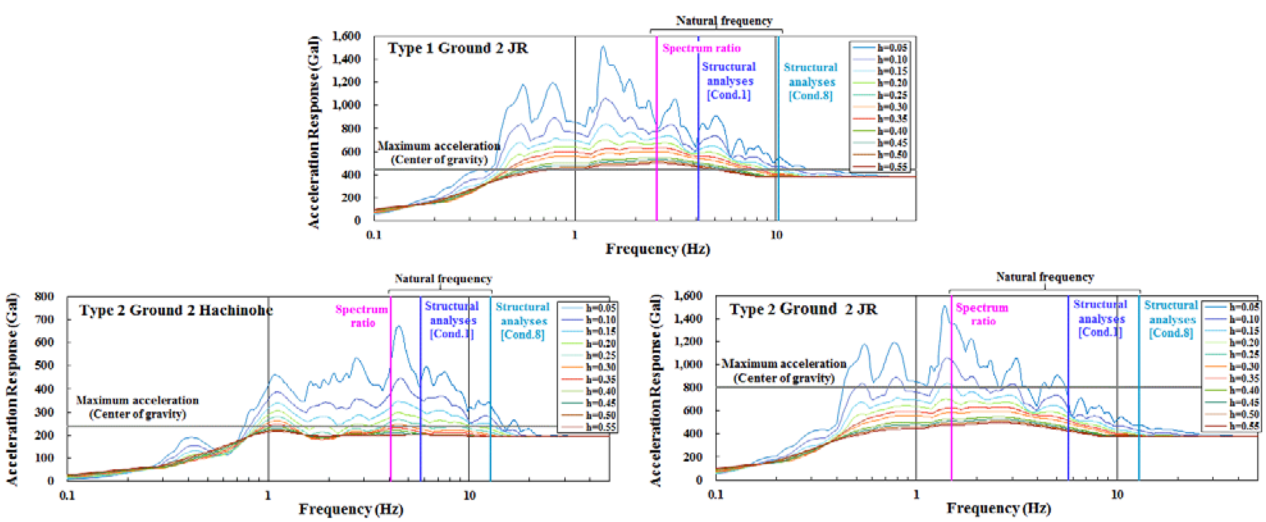

Fig.16 – Acceleration response spectrum

4. Conclusions

In this study, model testing and numerical analysis were carried out to establish a design method for evaluating coastal parapet levees' seismic performance taking their dynamic characteristics under earthquake loads into consideration. As a result, meaningful knowledge, mainly about the calculation of natural frequencies using a frame method and the estimation of maximum acceleration using acceleration response spectra, came to light.

The natural frequencies calculated by the experimental horizontal loading tests and structural frame analysis are similar to each other, and the applicability of the frame method for parapet levees was quite strongly supported. However, it is difficult for structural analysis to simulate the reduction of soil rigidity during earthquakes and the calculated natural frequencies of tall parapet walls like Type 2 were higher than expected. This is likely due to the position of center of gravity on the parapet wall. Although there were some gaps between the calculated natural frequencies, they did not affect the estimation of maximum acceleration by the response spectra, because the spectra were quite flat.

The experiments supported the applicability of the method estimating maximum acceleration using acceleration response spectra. In the numerical analysis, maximum accelerations estimated by the response spectra corresponded well with the measured maximum accelerations for Type 1. However, there were great disparities, particularly with large accelerations for Type 2. These inconsistencies, likely caused by rotation of the parapet levees, need to be studied further.

5. References

[1] Shore Protection Facility Technical Committee (2004): *Technical standards and commentary for shore protection facilities*, Japan Port Association (in Japanese).

[2] Ports and Harbours Bureau, Ministry of Land, Infrastructure, Transport and Tourism (2009): *Technical standards and commentaries for port and harbour facilities in Japan*, The Overseas Coastal Area Development Institute of Japan.

[3] Kumagai K, Watanabe Y, Nagao N and Ayugai M (2011): Field Survey of the 2011 off the Pacific Coast of Tohoku Earthquake and Tsunami on Shore Protection Facilities in Ports, *Technical Note of National Institute for Land and Infrastructure Management*, No.658, National Institute for Land and Infrastructure Management Ministry of Land, Infrastructure, Transport and Tourism, Japan (in Japanese).

[4] Kumagai K, Ehiro I, Asai T, Miyata M, Matsuda S, Washiya T and Kamaki M (2014): Field Survey of the 2011 off the Pacific Coast of Tohoku Earthquake and Tsunami on Shore Protection Facilities in Ports (II), *Technical Note of National Institute for Land and Infrastructure Management*, No.781, National Institute for Land and Infrastructure Management Ministry of Land, Infrastructure, Transport and Tourism, Japan (in Japanese).

[5] Asai T (2014): Characteristics of Damage of Coastal Protection Facilities in Ports due to the 2011 off the Pacific Coast of Tohoku Earthquake and Tsunami, *Technical Note of National Institute for Land and Infrastructure Management*, No.810, National Institute for Land and Infrastructure Management Ministry of Land, Infrastructure, Transport and Tourism, Japan (in Japanese).

[6] Japan Fishing Port Association (1998): *Handbook for fishing port and shore works* (in Japanese).

[7] Iwate prefectural land development section (2015): Structural drawing of construction of coastal levee and others in Atohama area of Ofunato port, retrieved October 29 2015, from http://www.pref.iwate.jp/nyuusatsu/sonota /038215.html (in Japanese).

[8] Iai S (1988): Similitude for shaking table tests on soil-structure model in 1G gravitational field. *Report of the port and harbor research institute*, **27**(3), 3-24, Ministry of Transport, Japan.

[9] Nagao T, Iwata N, Fujimura M, Morishita N, Sato H and Ozaki R (2006): Seismic coefficients of caisson type and sheet pile type quay walls. *Technical Note of National Institute for Land and Infrastructure Management*, No.310, National Institute for Land and Infrastructure Management Ministry of Land, Infrastructure, Transport and Tourism, Japan (in Japanese).

[10] Iai S, Matsunaga Y and Kameoka T (1990): Strain Space Plasticity Model for Cyclic Mobility. *Report of the Port and Harbour Research Institute*, **29**(4), 27-56, Ministry of Transport, Japan.

[11] Iai S, Matsunaga Y and Kameoka T (1992): Analysis of Undrained Cyclic Behavior of Sand under Anisotropic Consolidation. *Soil and Foundations*, **32**(2), 16-20.

[12] Morita T, Iai S, Liu H, Ichii K and Sato Y (1997): Simplified method to determine parameter of FLIP, *Technical note of the Port and Harbor Research Institute*, No.869, Ministry of Transport, Japan (in Japanese).

[13] Japan Road Association (2002): *Specifications and commentary for highway bridges*, Vol. I (in Japanese).

[14] Japan Road Association (2002): *Specifications and commentary for highway bridges*, Vol. IV (in Japanese).